POST-TEST ANALYSIS OF 3ET205 MODULE LC03TL12 FROM CHLORIDE MOTIVE POWER

Prepared for

Department of Energy
Office of Propulsion Systems
Electric and Hybrid Propulsion Division

and

Electric Power Research Institute
Customer Systems Division
Transportation Program

by

J. J. Marr, J. A. Smaga, and C. E. Webster

Argonne National Laboratory, Argonne, Illinois 60439
operated by The University of Chicago
for the United States Department of Energy

January 1992

Argonne National Laboratory, with facilities in the states of Illinois and Idaho, is owned by the United States government, and operated by The University of Chicago under the provisions of a contract with the Department of Energy under Contract W-31-109-Eng-38.

ANL/RP--75379

DE92 009723

Battery History

ANL's Analysis and Diagnostics Laboratory conducted a SFUDS life evaluation on a 3ET205 lead-acid module from Chloride Motive Power of England. Like other 3ET205 modules, module LC03TL12 consisted of three cells with tubular positive electrodes as the primary design feature. Testing began with an abbreviated performance characterization of 28 cycles. The module achieved a specific energy of 34.6 Wh/kg for 3-h discharges and a 30-s peak power of 90 W/kg at 50% depth of discharge (DOD). These values were consistent with previously tested modules of this design. The characterization phase was followed by evaluation on a modified SFUDS regime to 100% DOD. The modification was a 400-A limit to prevent excessive voltage depression during the high-power steps in the SFUDS algorithm.

The SFUDS evaluation is summarized in Fig. 1. The module maintained a net specific energy at or near 27.6 Wh/kg (32.7 Wh/kg if regenerative braking is included) over the first 110 cycles and then began to decline abruptly. The end-of-life criteria, 80% of initial SFUDS energy, occurred on cycle 149. A series of constant-current discharges at this point effected a partial recovery in capacity from 85 to 92% of the initial 191 Ah at the 3-h rate. The module was returned to SFUDS cycling on cycle 162, but testing was officially terminated after 167 cycles, when the specific energy again declined below 80%. Resistance measurements made throughout the evaluation revealed an accelerating increase in internal resistance. Module LC03TL12 was then placed on float charge for two months, and following a few cycles of constant-current discharge, it was subjected to cell-level diagnostic tests. These tests formed part of a post-test analysis which also included teardown and examination of selected electrode materials.

Diagnostic Testing

Individual cell potentials and half-cell potentials were measured for each cell in module LC03TL12. The individual cell potentials are overlaid in Fig. 2. These measurements revealed that cell 1, the cell containing the module's negative terminal, had the lowest cell voltage among the cells throughout the finishing charge and most of the discharge. Cell 2, however, actually dropped to the lowest voltage by the very end of discharge and limited the module's capacity. Reference electrode measurements were performed on all three cells, and the results are illustrated in Figs. 3, 4, and 5 for cells 1, 2, and 3, respectively. From these voltage traces, the low voltage for cell 1 was attributed to the depressed voltage response of the negative electrodes. In all three cells, the negative electrodes played a major role in limiting cell capacity, especially for cell 1. The positive electrodes of cell 2, however, also contributed to the capacity decline of this cell.

Teardown and Examination Findings

Module LC03TL12 was returned to the charged state prior to teardown and examination. The appearance of all three cells was found to be similar after the module lid was removed. All three cells were examined. The results are summarized below.

Cell Hardware:

No mechanical defects were evident. The internal connections were sound and featured good fusion of the electrode tabs to the internal bus bars. Corrosion of the positive buses produced a thick, loose, dark-brown layer over the surfaces. Subsequent analysis found the layer to be composed of PbO_2 and $PbSO_4$.

Each cell contained a plastic comb over the top of the negative electrode stack. This new feature was effective in preventing the formation of particulate bridges along the tops of adjacent electrodes. The comb kept spalled corrosion products from the positive bus off the negative electrodes and contained mossy, lead deposits within the vicinity of the originating negative electrode.

The separators were in excellent condition. No physical deterioration or active material penetration was observed for the separators from any cell.

Electrolyte specific gravity was measured for all cells, and the values range from 1.336 to 1.346 g/cc. The highest value was for cell 2 and was higher than normally observed for this technology. The solution densities are listed in Table 1, which provides a summary of the measurements made for all three cells.

Positive Electrodes:

The positive electrodes from all three cells were in comparable condition. As shown in Fig. 6, growth of the positive electrodes was evident. The width of these electrodes at mid-height had increased by 0.4 to 0.7 cm when compared to measurements made at the base. Growth was greatest for central electrodes, presumably because of the better constraint imposed on the outer electrodes by the walls of the cell case. In general, the positive electrode gauntlets used in this tubular design were effective in retaining the active material in place. Loss of positive active material (PAM) was generally restricted to the bottom 1 cm of the six outermost tubes of the 30-tube gauntlet. Shed active materials were collected from the bottom of the cells and weighed. As shown in Table 1, the collected material weighed progressively less in ascending cell order. The 136 g from cell 1 was still lower than seen in past examinations of this technology.

When examined in detail, no significant degradation of the PAM was identified. Intrusion porosimetry of electrode samples from cell 1 indicated a minor loss in pore volume. Scanning electron microscopy showed that the morphology of the PAM in all three cells was normal. As illustrated in Fig. 7, the active materials consisted of closed packed aggregates of fine-grained PbO_2. Neither a coralloid structure of PbO_2 nor $PbSO_4$ crystals were found in the examined sections.

The most noticeable difference for the positive electrodes was in the condition of the positive grids, i.e., the central wire in each tubular electrode section. Metallograpic examination of the wires in cross section revealed that corrosion ranged from moderate in cell 1 to mild in cell 3. As shown in Fig. 8, the grid wire from these cells ranged from 1.8 to 2.4

mm^2 in cross-sectional area. These reductions were accompanied by the development of corresponding corrosion layers that reached thicknesses of 200 to 50 μm. Corrosion of the grid wires in cell 2 was intermediate between these extremes. The corrosion layers appeared relatively crack-free and adherent to the lead-alloy substrate.

TABLE 1. Summary of Analytical Findings for Module LC03TL12

Cell Number	1	2	3
Sol'n. Density (g/cc)	1.337	1.346	1.336
Shed Material (g)	136	121	113
Pos. Grid Cross Sec. Area (mm^2)	1.?	2.2	2.4
Pos. Grid Cor. Layer (μm)	200	80	50
Pos. Pore Volume (cc/g)	0.160	---	---
Neg. Pore Volume (cc/g)	0.204	0.209	0.211
Sb in NAM (ppm)			
- surface	2610	1280	1230
- core	610	370	440

Negative Electrodes:

The negative electrodes from these cells showed visible signs of degradation. As a group, they were dull in appearance. The surface material was softened and possessed little metallic sheen when scraped. The perimeters of these electrodes had developed deposits of mossy lead that ranged from 0.1 to 0.3 cm in height. The bulk of these deposits was concentrated along the top edges of the electrode. Subsequent microscopic study found some degree of sulfation. For cells 2 and 3, the $PbSO_4$ crystals were located in the electrode surfaces (Fig. 9). In cell 1, small $PbSO_4$ crystals were also identified in the core of the electrodes (Fig. 10). The morphology of these electrodes, however, retained an open skeletal structure. In addition, the porosity values for these electrodes were quite good, exceeding 0.2 cc/g for all three cells.

An important finding for the negative electrodes was high concentrations of antimony, especially for the negative active material (NAM) taken from cell 1. Spectrochemical analysis was performed on samples from the core and from the surface of electrodes from each cell.

As shown in Table 1, the antimony concentrations were especially high for the electrode surfaces (~12 J to 2600 ppm). The core concentrations were roughly one-fourth to one-third as high, but these values were still above the threshold for antimony "poisoning," i.e., the concentration required to severely depress the hydrogen overvoltage and cause excessive hydrolysis.

The grids in the negative electrodes were intact and free of corrosion. The adhesion between the NAM and the grids was found to be very good, as illustrated in Fig. 11.

Conclusions

The results of the post-test investigation of module LC03TL12 indicated that the immediate cause of capacity decline of the module was antimony poisoning of the negative electrodes. High concentrations were found in all NAM samples, especially the samples from cell 1. The concentrations were sufficient to reduce the charging efficiency and thereby decrease the effective capacity of the module. The depressed negative-electrode voltage trace for cell 1 was consistent with excessive electrolysis due to a reduced hydrogen overvoltage. In most other respects, the negative electrodes were in generally sound condition.

Corrosion of the positive grid wires served as the ultimate source of the performance decline. The Sb-Pb alloy used for these grids proved to be primary source of antimony. The analytical data showed a strong correlation between the degree of positive grid corrosion and the antimony levels in the corresponding negative electrodes. Grid corrosion also was the primary source of increased internal resistance. The effective reduction in cross-sectional area for the grid wires and the thick corrosion scales led to the progressive resistance rise noted during the evaluation. This factor was especially critical in an SFUDS evaluation because maintenance of adequate power is essential to longevity. In comparison to some other lead-acid technologies, the 3ET205 design begins at a power disadvantage and can ill afford additional power losses with cycling.

This examination also provided the opportunity for comparison with the findings for another 3ET205 module that was evaluated primarily on the J227aC profile for a G-Van. The module, designated LC03TL11, achieved 715 cycles to 100% DOD before reaching end-of-life. The cause of failure for module LC03TL11 was also found to be antimony poisoning of the negative electrodes due to corrosion of the positive electrode grids. In fact, the maximum contamination levels were ~2600 ppm for both modules. In general, degradation of module LC03TL11 was more pronounced in the following areas: degree of positive grid corrosion, shed PAM, the average Sb levels in the NAM, losses in NAM pore volume and grid adhesion, the amount of mossy Pb deposits at the perimeter of the negative electrodes, and the level of sulfation of the negative electrode surfaces.

The failure of module LC03TL12 may seem somewhat premature in view of the approximately 4.5 times longer life of module LC03TL11. We interpret the spread in cycle life as a combination of two factors. First is the difference in peak power demands, 79 W/kg for SFUDS versus 36 W/kg for the G-van profile. The SFUDS algorithm would be expected to have a major impact on the power-limited 3ET205 design. Second, the cells of module

LC03TL11 appeared to be better matched in comparison to the cells used for module LC03TL12. For example, the three cells of module LC03TL12 showed a wider divergence in post-test findings than the cells for module LC03TL11. Also, cell 1 was noted to consume more water early in the evaluation of module LC03TL12. Thus, the possibility existed that a marginal cell impaired the SFUDS evaluation of this module.

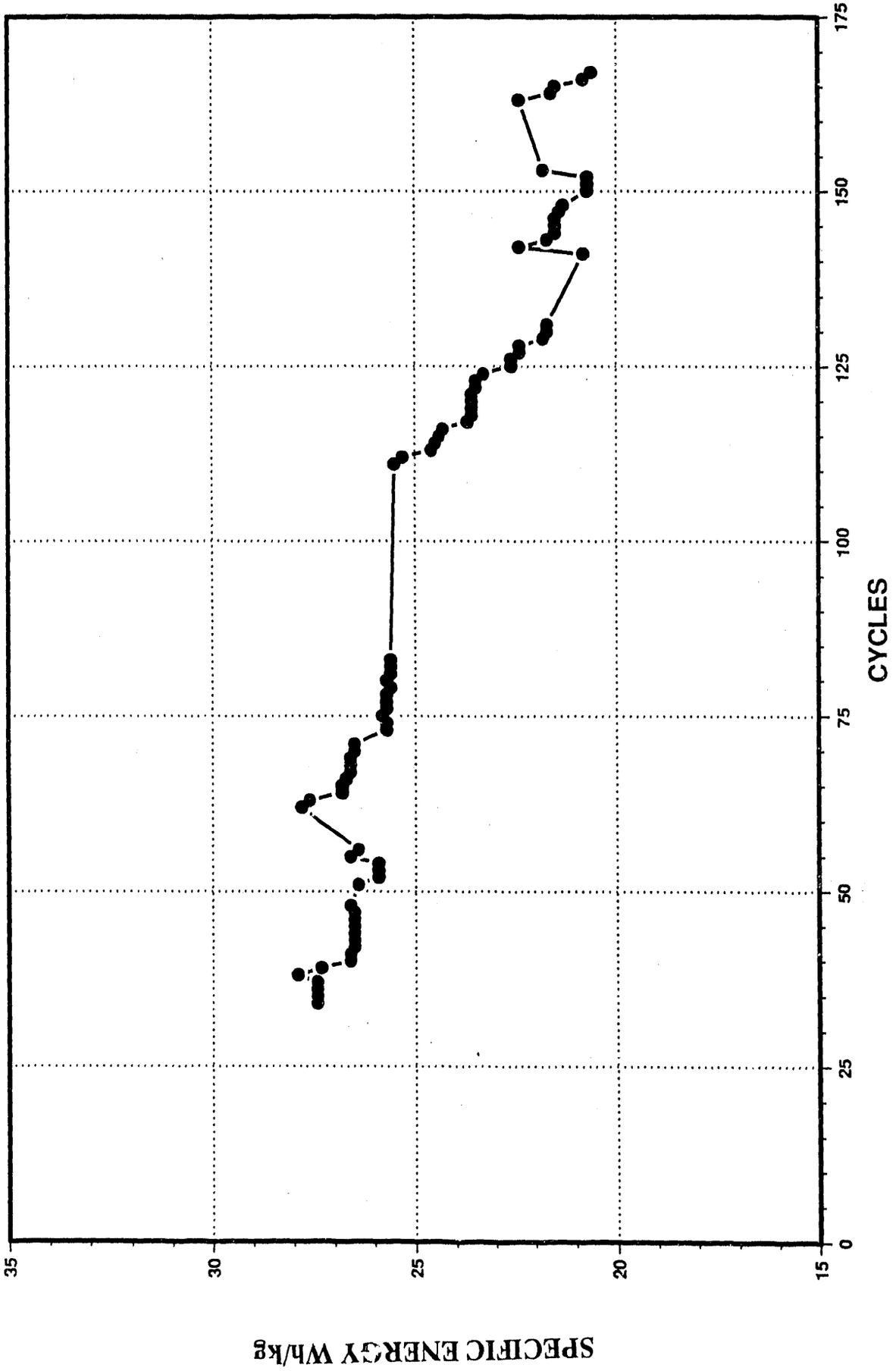

Fig. 1. Net Specific Energy History of 3ET205 Module LC03TL12 for SFUDS Cycles

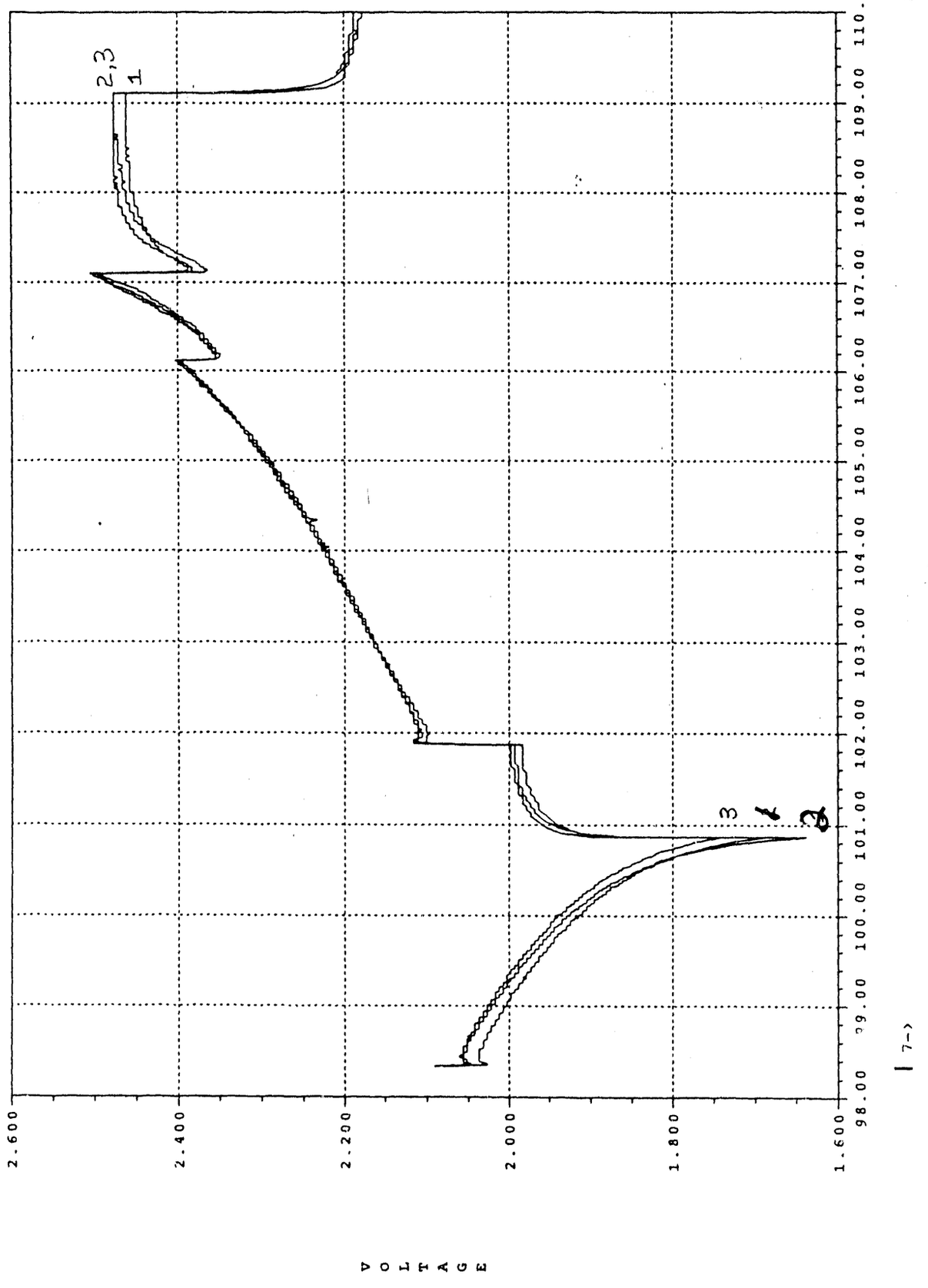

Fig. 2. Overlaid Voltage (in volts) Traces for the Three Cells of Module LC03TL12 during Cycle 174

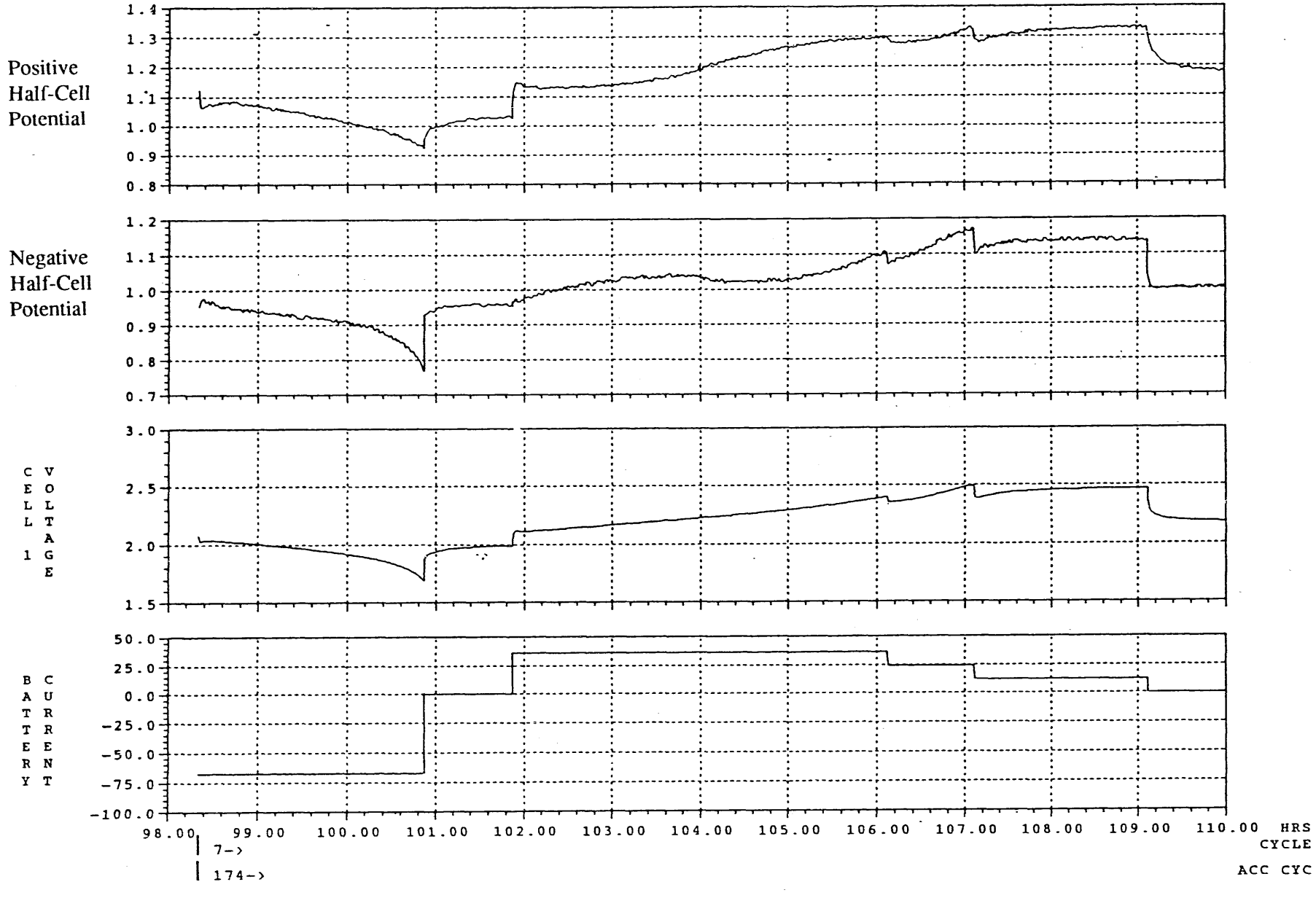

Fig. 3. Reference Electrode Measurements for Cell 1 in Module LC03TL12 during Cycle 174

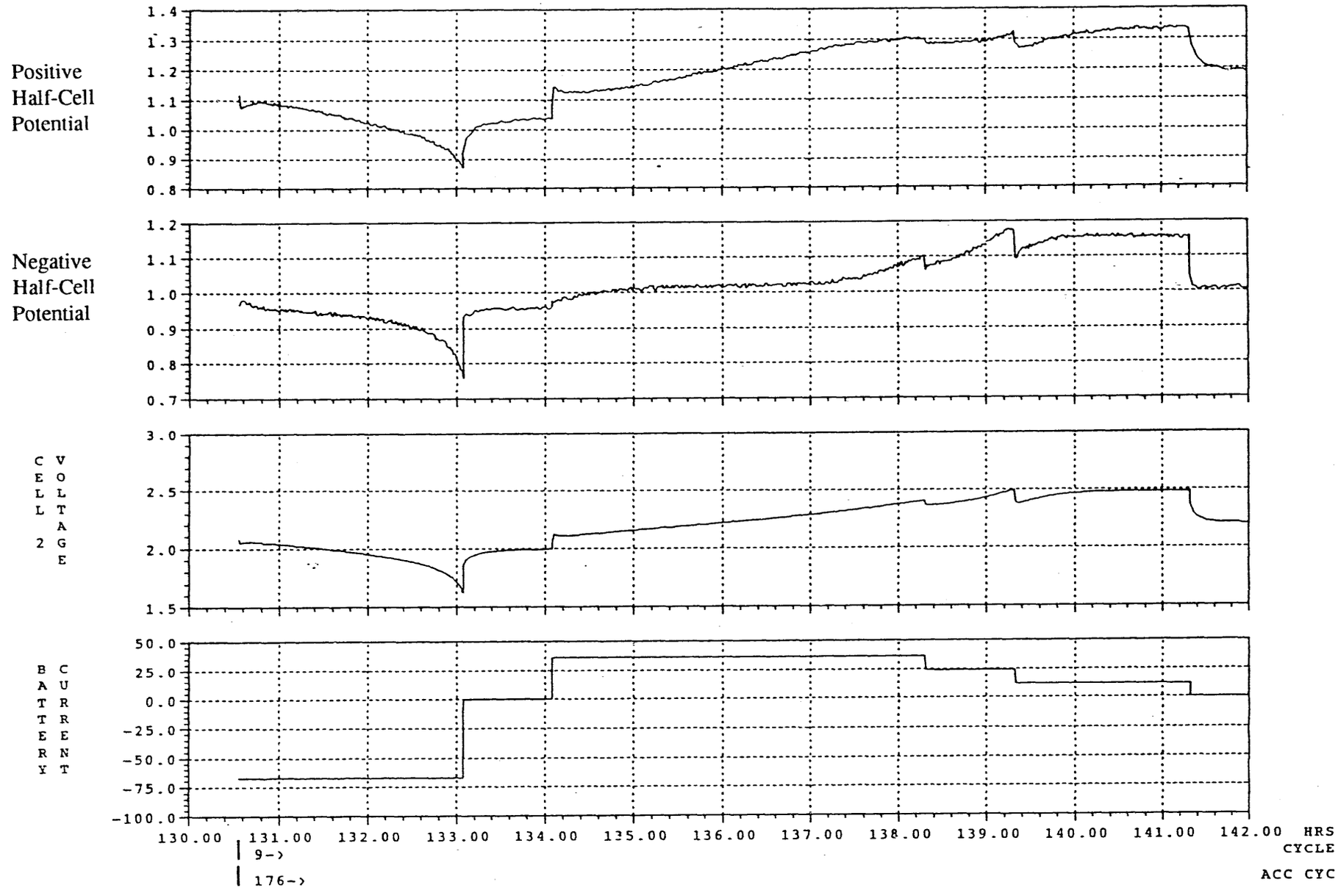

Fig. 4. Reference Electrode Measurements for Cell 2 in Module LC03TL12 during Cycle 176

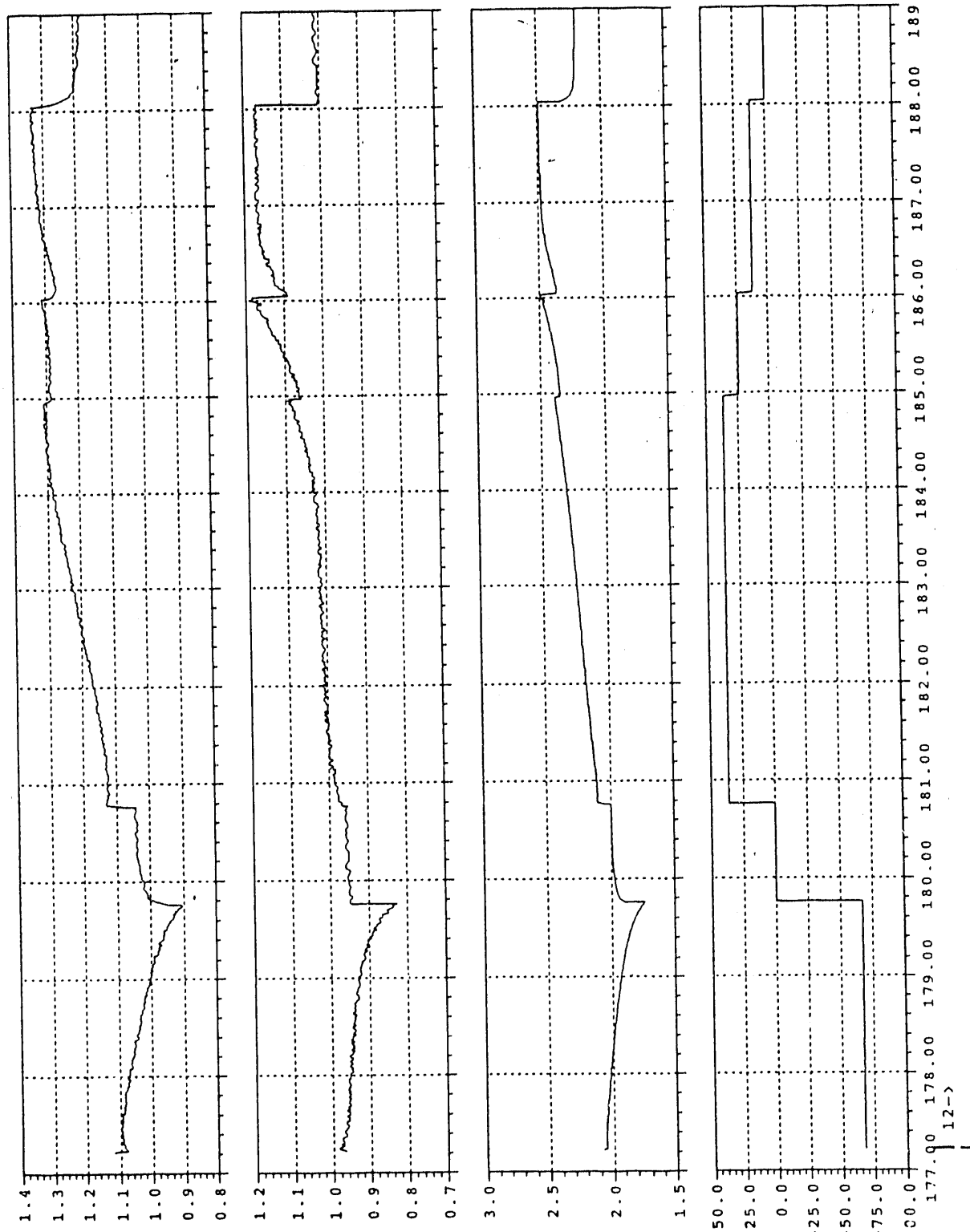

Fig. 5. Reference Electrode Measurements for Cell 3 in Module LC03TL12 during Cycle 179

Fig. 6. Typical Positive Electrode from Cell 1

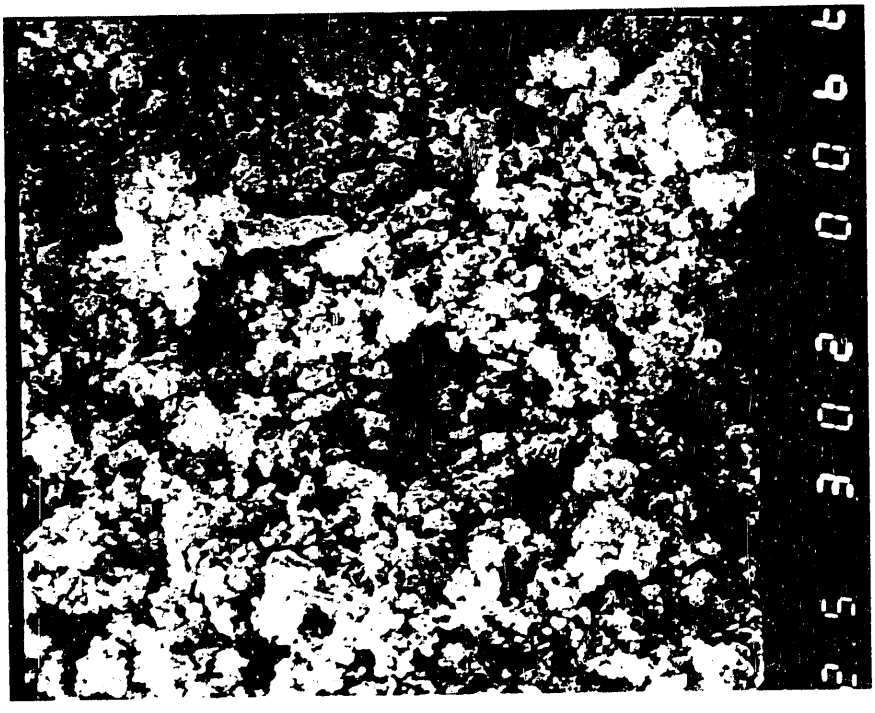

Fig. 7. Microstructure of PAM from Cell 1 (3000X)

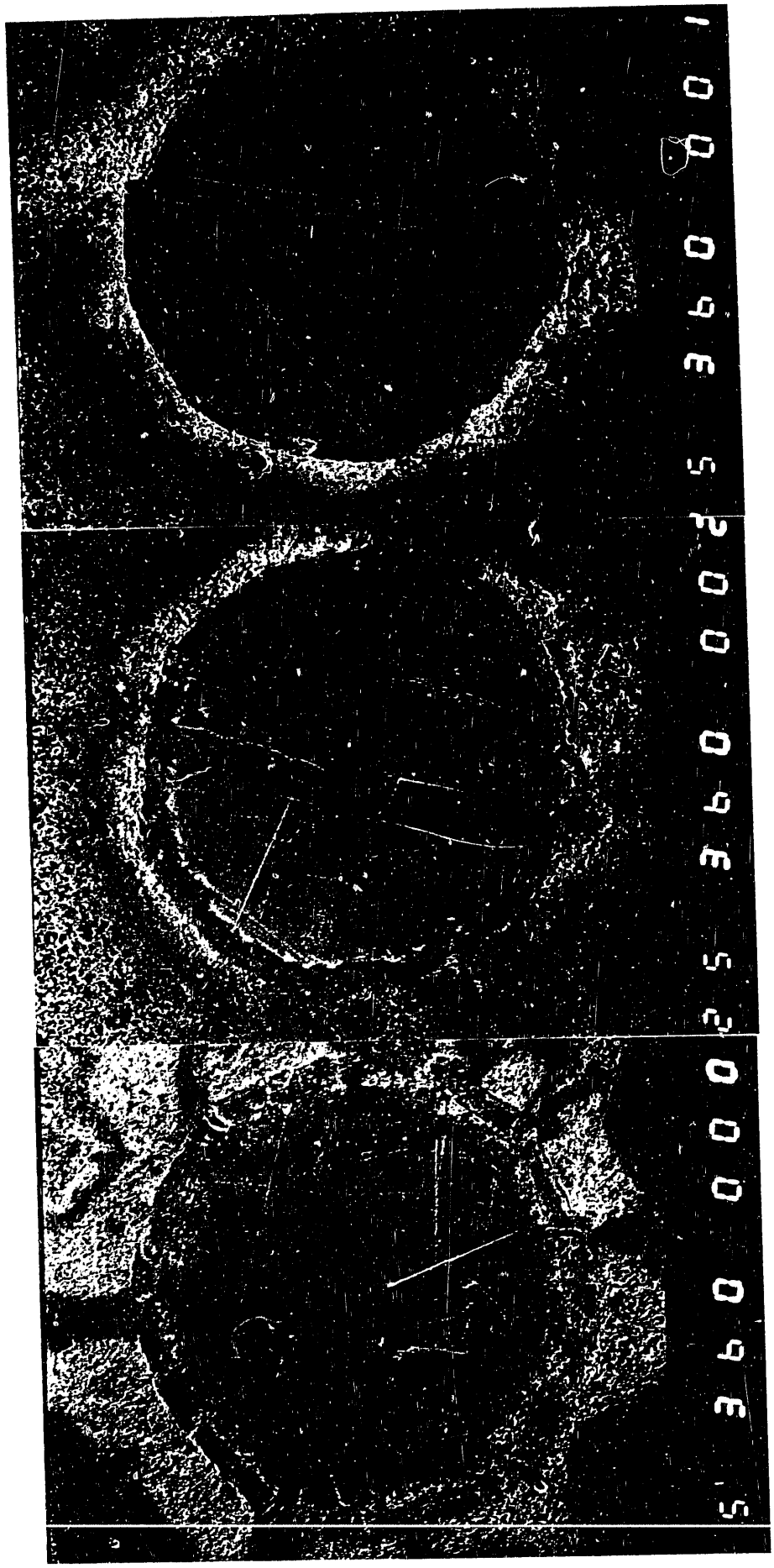

Fig. 8. Positive Grid Wires in Cross Section (36X)
Left Cell 1
Center Cell 2
Right Cell 3

Fig. 9. Lead Sulfate Crystals on the Surface of a Negative Electrode (3000X)

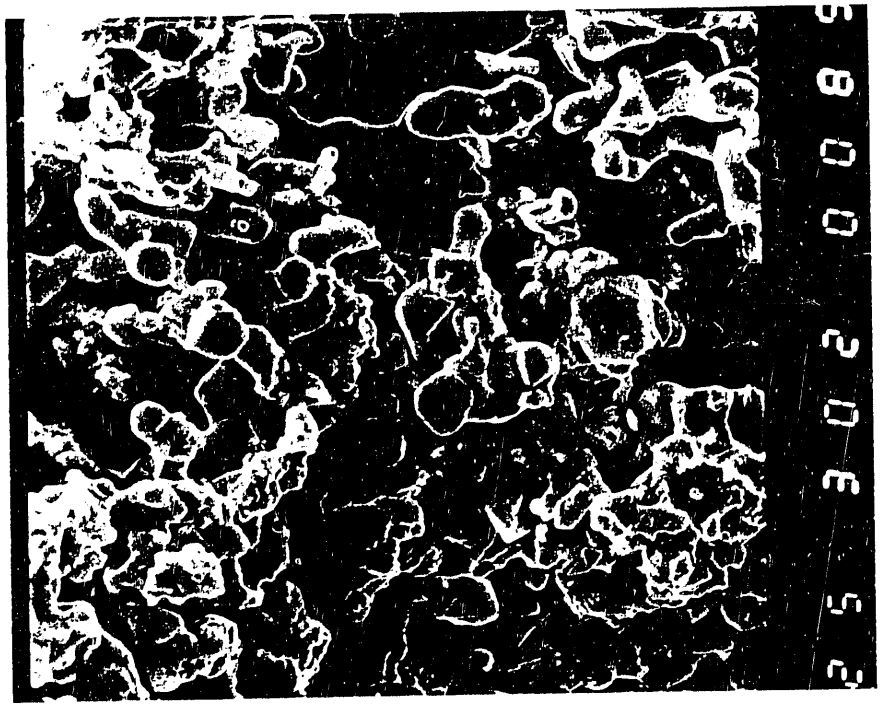

Fig. 10. Microstructure of NAM from the Core of Cell 1 (3000X)

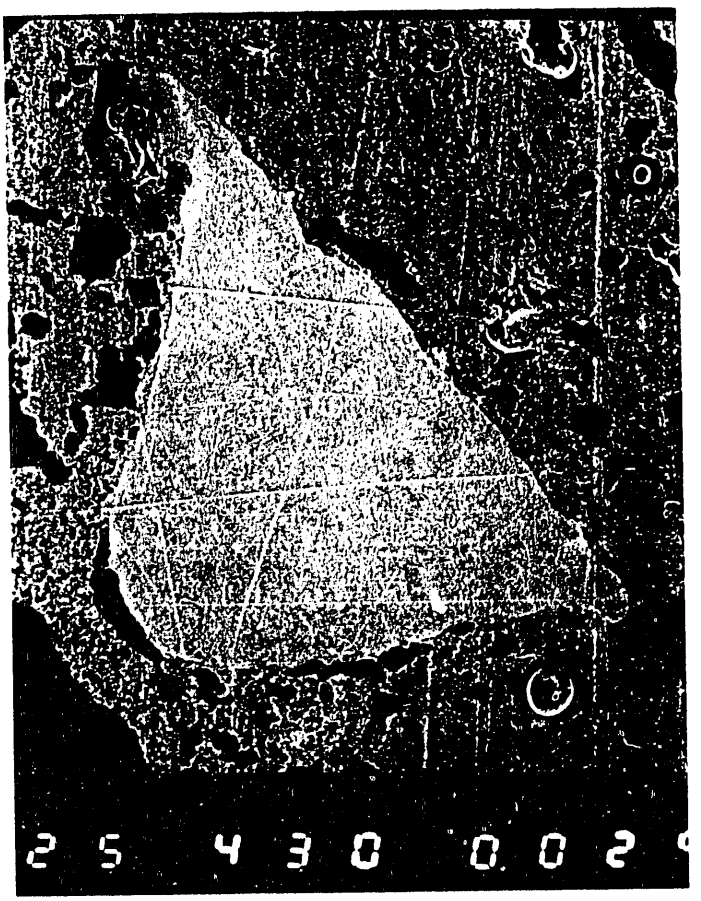

Fig. 11. Negative Grid Element in Cross Section (43X)

END

DATE FILMED

4/21/92